ELSEVIER

Comput. Methods Appl. Mech. Engrg. 123 (1995) 1–13

Computer methods in applied mechanics and engineering

Pseudo-transient large deflection analysis of composite and sandwich shells with a refined theory

J.R. Kommineni, T. Kant*

Department of Civil Engineering, Indian Institute of Technology, Powai, Bombay-400 076, India

Received 5 August 1992; revised manuscript received 16 November 1994

Abstract

An unified approach is presented for linear and geometrically non-linear analyses of composite and sandwich shells with a refined theory and C^0 finite elements by using the dynamic relaxation technique. A finite element idealization with a nine noded quadrilateral isoparametric element belonging to the Lagrangian family is used in space discretization. An explicit time stepping scheme is employed for time integration of the resulting discrete ordinary differential equations with special forms of diagonal fictitious mass and/or damping matrices. The accuracy of the formulation is then established by comparing the present pseudo-transient (PT) analysis results with the available 2D/3D analytical and finite element solutions. The usefulness and effectiveness of this approach is established by comparing computational time required by this and Newton–Raphson's (NR) approaches.

1. Introduction

Structural elements made up of fibre reinforced composite materials are being extensively used in high and low technology areas in recent years. Their industrial applications are multiplying rapidly because of their superior mechanical properties. Because of high modulus and high strength properties that composites have, structural composites undergo large deformations before they become inelastic. Therefore, an accurate prediction of displacements and stresses are possible only when one accounts the geometric non-linearity. The partial differential equations describing the large deflection behavior of anisotropic composite shells of arbitrary geometry are not amenable to classical analytical methods. The finite element method has proved to be a very powerful tool for analyzing structural problems, involving complex geometries, loadings, boundaries and non-linearities.

In this paper a unified approach for the static, both linear and geometrically non-linear, elastic analyses of laminated composite and sandwich shells is presented which employs a refined theory and C^0 finite elements.

2. Theory

The laminate considered here is composed of a finite number of orthotropic layers, with principal material axes of elasticity oriented arbitrarily with respect to the laminate axes. The x, y coordinates of

* Corresponding author.

SSDI 0045-7825(94)00771-3

the laminate are taken at the mid-surface of the shell (see Fig. 1) and the displacement model is assumed as,

$$\begin{aligned} u(x, y, z, t) &= u_0(x, y, t) + z\theta_x(x, y, t) + z^2 u_0^*(x, y, t) + z^3\theta_x^*(x, y, t) \\ v(x, y, z, t) &= v_0(x, y, t) + z\theta_y(x, y, t) + z^2 v_0^*(x, y, t) + z^3\theta_y^*(x, y, t) \\ w(x, y, z, t) &= w_0(x, y, t) \end{aligned} \tag{1}$$

where t represents time, the terms u, v and w are the displacement components of a general point (x, y, z) in the laminate domain in the x, y and z directions, respectively. The parameters u_0 and v_0 are the tangential displacement components and w_0 is the transverse displacement component of a point (x, y) on the middle surface. The functions θ_x and θ_y are rotations of the normals to the middle surface about y and x axes, respectively. The parameters u_0^*, v_0^*, θ_x^* and θ_y^* are the higher-order terms in the Taylor's series expansion and they represent higher-order transverse cross-sectional deformation modes which are also defined at mid-surface.

In the present investigation, large displacements in the sense of von Karman assumptions, which in particular imply that the first-order derivatives of tangential displacement components with respect to x, y and z are small, so that their particular products can be neglected are considered. The following are the strain–displacement relations

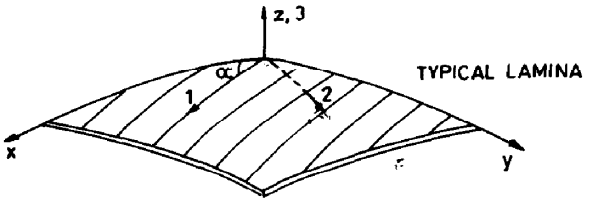

(1, 2, 3) - LAMINA REFERENCE AXES

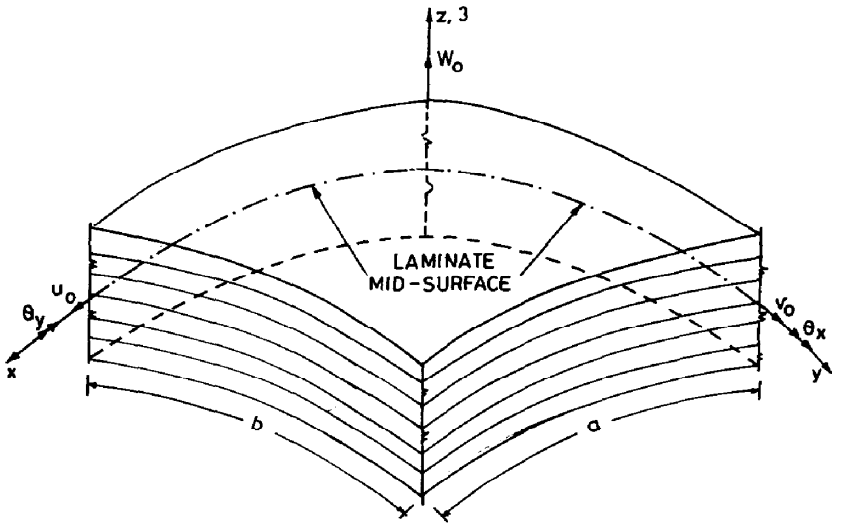

(x, y, z) - LAMIATE REFERENCE AXES

Fig. 1. Laminated shell geometry with positive set of lamina/laminate reference axes, displacement components and fibre orientation.

$$
\begin{aligned}
\varepsilon_x &= \frac{\partial u}{\partial x} + \frac{w}{R_1} + \frac{1}{2}\left(\frac{\partial w}{\partial x}\right)^2 \\
\varepsilon_y &= \frac{\partial v}{\partial y} + \frac{w}{R_2} + \frac{1}{2}\left(\frac{\partial w}{\partial y}\right)^2 \\
\gamma_{xy} &= \frac{\partial u}{\partial y} + \frac{\partial v}{\partial x} + \frac{\partial w}{\partial x}\cdot\frac{\partial w}{\partial y} \\
\gamma_{zx} &= \frac{\partial u}{\partial z} + \frac{\partial w}{\partial x} - \frac{u}{R_1} \\
\gamma_{yz} &= \frac{\partial v}{\partial z} + \frac{\partial w}{\partial y} - \frac{v}{R_2}
\end{aligned}
\tag{2}
$$

The stress–strain relations for a typical layer L with reference to the laminate axes (x, y, z) after the usual transformation of stresses/strains between the lamina and laminate coordinate system are

$$\boldsymbol{\sigma} = \boldsymbol{Q}\boldsymbol{\varepsilon} \tag{3a}$$

in which $\boldsymbol{\sigma} = (\sigma_x,\ \sigma_y,\ \tau_{xy},\ \tau_{xz},\ \tau_{yz})^t$ is stress vector and $\boldsymbol{\varepsilon} = (\varepsilon_x,\ \varepsilon_y,\ \gamma_{xy},\ \gamma_{xz},\ \gamma_{yz})^t$ is strain vector with respect to laminate axes, the superscript 't' indicates the transpose of matrix/vector and the elements of Q matrix are defined as follows

$$\boldsymbol{Q} = \begin{bmatrix} \boldsymbol{Q}_{ij} & \boldsymbol{0} \\ \boldsymbol{0} & \boldsymbol{Q}_{lm} \end{bmatrix};\quad \begin{matrix} i, j = 1, 2, 3 \\ l, m = 4, 5 \end{matrix} \tag{3b}$$

in which

$$
\begin{aligned}
Q_{11} &= C_{11}\cdot c^4 + (2\cdot C_{12} + 4\cdot C_{33})\cdot s^2\cdot c^2 + C_{22}\cdot s^4 \\
Q_{12} &= C_{12}\cdot(c^4 + s^4) + (C_{11} + C_{22} - 4\cdot C_{33})\cdot s^2\cdot c^2 \\
Q_{13} &= (C_{11} - C_{12} - 2\cdot C_{33})\cdot s\cdot c^3 + (C_{12} - C_{22} + 2\cdot C_{33})\cdot s^3\cdot c \\
Q_{22} &= C_{11}\cdot s^4 + (2\cdot C_{12} + 4\cdot C_{33})\cdot s^2\cdot c^2 + C_{22}\cdot c^4 \\
Q_{23} &= (C_{11} - C_{12} - 2\cdot C_{33})\cdot s^3\cdot c + (C_{12} - C_{22} + 2\cdot C_{33})\cdot s\cdot c^3 \\
Q_{33} &= C_{33}\cdot(c^4 + s^4) + (C_{11} - 2\cdot C_{12} + C_{22} - 2\cdot C_{33})\cdot s^2\cdot c^2 \\
Q_{44} &= C_{44}\cdot c^2 + C_{55}\cdot s^2 \\
Q_{45} &= (C_{44} - C_{55})\cdot c\cdot s \\
Q_{55} &= C_{44}\cdot s^2 + C_{55}\cdot c^2
\end{aligned}
\tag{3c}
$$

The laminate constitutive relations involving membrane forces, bending moments and shear forces are defined as

$$
\begin{aligned}
\begin{bmatrix} N_x & N_x^* \\ N_y & N_y^* \\ N_{xy} & N_{xy}^* \end{bmatrix} &= \sum_{L=1}^{\mathrm{NL}} \int_{z_L}^{z_{L+1}} \begin{bmatrix} \sigma_x \\ \sigma_y \\ \tau_{xy} \end{bmatrix} [1,\quad z^2]\,\mathrm{d}z \\
\begin{bmatrix} M_x & M_x^* \\ M_y & M_y^* \\ M_{xy} & M_{xy}^* \end{bmatrix} &= \sum_{L=1}^{\mathrm{NL}} \int_{z_L}^{z_{L+1}} \begin{bmatrix} \sigma_x \\ \sigma_y \\ \tau_{xy} \end{bmatrix} [z,\quad z^3]\,\mathrm{d}z \\
\begin{bmatrix} Q_x & Q_x^* & S_x & S_x^* \\ Q_y & Q_y^* & S_y & S_y^* \end{bmatrix} &= \sum_{L=1}^{\mathrm{NL}} \int_{z_L}^{z_{L+1}} \begin{bmatrix} \tau_{xz} \\ \tau_{yz} \end{bmatrix} [1,\quad z^2,\quad z,\quad z^3]\,\mathrm{d}z
\end{aligned}
\tag{4a}
$$

Upon integration, these expressions are rewritten in a matrix form which defines the stress-resultant and mid-surface strain relationship of a composite shell [1] and is given by

$$\bar{\boldsymbol{\sigma}} = \boldsymbol{D}\bar{\boldsymbol{\varepsilon}} \tag{4b}$$

$$\begin{bmatrix} \boldsymbol{N} \\ \boldsymbol{M} \\ \boldsymbol{Q} \end{bmatrix} = \begin{bmatrix} \boldsymbol{D}_{\mathrm{m}} & \boldsymbol{D}_{\mathrm{c}} & \boldsymbol{0} \\ \boldsymbol{D}_{\mathrm{c}}^{\mathrm{t}} & \boldsymbol{D}_{\mathrm{b}} & \boldsymbol{0} \\ \boldsymbol{0} & \boldsymbol{0} & \boldsymbol{D}_{\mathrm{s}} \end{bmatrix} \begin{bmatrix} \boldsymbol{\varepsilon}_{\mathrm{m}} \\ \boldsymbol{\varepsilon}_{\mathrm{b}} \\ \boldsymbol{\varepsilon}_{\mathrm{s}} \end{bmatrix} \tag{4c}$$

where $\boldsymbol{N}^{\mathrm{t}} = [N_x,\ N_y,\ N_{xy},\ N_x^*,\ N_y^*,\ N_{xy}^*]$; $\boldsymbol{M}^{\mathrm{t}} = [M_x,\ M_y,\ M_{xy},\ M_x^*,\ M_y^*,\ M_{xy}^*]$ and $\boldsymbol{Q}^{\mathrm{t}} = [Q_x,\ Q_y,\ Q_x^*,\ Q_y^*,\ S_x,\ S_y,\ S_x^*,\ S_y^*]$ and the stiffness coefficient matrices $\boldsymbol{D}_{\mathrm{m}}, \boldsymbol{D}_{\mathrm{c}}, \boldsymbol{D}_{\mathrm{b}}, \boldsymbol{D}_{\mathrm{s}}$ are defined as follows

$$\boldsymbol{D}_{\mathrm{m}} = \sum_{L=1}^{\mathrm{NL}} \begin{bmatrix} \boldsymbol{Q}_{ij}H_1 & \boldsymbol{Q}_{ij}H_3 \\ \boldsymbol{Q}_{ij}H_3 & \boldsymbol{Q}_{ij}H_5 \end{bmatrix}; \qquad \boldsymbol{D}_{\mathrm{c}} = \sum_{L=1}^{\mathrm{NL}} \begin{bmatrix} \boldsymbol{Q}_{ij}H_2 & \boldsymbol{Q}_{ij}H_4 \\ \boldsymbol{Q}_{ij}H_4 & \boldsymbol{Q}_{ij}H_6 \end{bmatrix} \tag{4d}$$

$$\boldsymbol{D}_{\mathrm{b}} = \sum_{L=1}^{\mathrm{NL}} \begin{bmatrix} \boldsymbol{Q}_{ij}H_3 & \boldsymbol{Q}_{ij}H_5 \\ \boldsymbol{Q}_{ij}H_5 & \boldsymbol{Q}_{ij}H_7 \end{bmatrix}; \qquad \boldsymbol{D}_{\mathrm{s}} = \sum_{L=1}^{\mathrm{NL}} \begin{bmatrix} \boldsymbol{Q}_{lm}H_1 & \boldsymbol{Q}_{lm}H_3 & \boldsymbol{Q}_{lm}H_2 & \boldsymbol{Q}_{lm}H_4 \\ \boldsymbol{Q}_{lm}H_3 & \boldsymbol{Q}_{lm}H_5 & \boldsymbol{Q}_{lm}H_4 & \boldsymbol{Q}_{lm}H_6 \\ \boldsymbol{Q}_{lm}H_2 & \boldsymbol{Q}_{lm}H_4 & \boldsymbol{Q}_{lm}H_3 & \boldsymbol{Q}_{lm}H_5 \\ \boldsymbol{Q}_{lm}H_4 & \boldsymbol{Q}_{lm}H_6 & \boldsymbol{Q}_{lm}H_5 & \boldsymbol{Q}_{lm}H_7 \end{bmatrix} \tag{4e}$$

In the above relations $i, j = 1, 2, 3$ and $l, m = 4, 5$ and $H_k = (z_{L+1}^k - z_L^k)/k$, $k = 1, 2, 3, 4, 5, 6, 7$ and NL is the number of layers and $\bar{\boldsymbol{\varepsilon}} = (\bar{\boldsymbol{\varepsilon}}_{\mathrm{m}}^{\mathrm{t}},\ \bar{\boldsymbol{\varepsilon}}_{\mathrm{b}}^{\mathrm{t}},\ \bar{\boldsymbol{\varepsilon}}_{\mathrm{s}}^{\mathrm{t}})^{\mathrm{t}}$ represents the mid-surface membrane, bending and shear strain components, respectively and are defined as follows

$$\bar{\boldsymbol{\varepsilon}}_{\mathrm{m}} = \begin{bmatrix} \dfrac{\partial u_0}{\partial x} + \dfrac{w_0}{R_1} + \dfrac{1}{2}\left(\dfrac{\partial w_0}{\partial x}\right)^2 \\ \dfrac{\partial v_0}{\partial y} + \dfrac{w_0}{R_2} + \dfrac{1}{2}\left(\dfrac{\partial w_0}{\partial y}\right)^2 \\ \dfrac{\partial v_0}{\partial x} + \dfrac{\partial u_0}{\partial y} + \dfrac{\partial w_0}{\partial x}\cdot\dfrac{\partial w_0}{\partial y} \\ \dfrac{\partial u_0^*}{\partial y} \\ \dfrac{\partial v_0^*}{\partial x} \\ \dfrac{\partial v_0^*}{\partial x} + \dfrac{\partial u_0^*}{\partial y} \end{bmatrix}; \qquad \bar{\boldsymbol{\varepsilon}}_{\mathrm{b}} = \begin{bmatrix} \dfrac{\partial \theta_x}{\partial x} \\ \dfrac{\partial \theta_y}{\partial y} \\ \dfrac{\partial \theta_y}{\partial x} + \dfrac{\partial \theta_x}{\partial y} \\ \dfrac{\partial \theta_x^*}{\partial x} \\ \dfrac{\partial \theta_y^*}{\partial y} \\ \dfrac{\partial \theta_y^*}{\partial x} + \dfrac{\partial \theta_x^*}{\partial y} \end{bmatrix}; \qquad \bar{\boldsymbol{\varepsilon}}_{\mathrm{s}} = \begin{bmatrix} \theta_x + \dfrac{\partial w_0}{\partial x} - \dfrac{u_0}{R_1} \\ \theta_y + \dfrac{\partial w_0}{\partial y} - \dfrac{v_0}{R_2} \\ 3\theta_x^* - \dfrac{u_0^*}{R_1} \\ 3\theta_y^* - \dfrac{v_0^*}{R_2} \\ 2u_0^* - \dfrac{\theta_x}{R_1} \\ 2v_0^* - \dfrac{\theta_y}{R_2} \\ -\dfrac{\theta_x^*}{R_1} \\ -\dfrac{\theta_y^*}{R_2} \end{bmatrix} \tag{4f}$$

and

$$\bar{\boldsymbol{\varepsilon}}^{\mathrm{t}} = (\bar{\boldsymbol{\varepsilon}}_{\mathrm{m}}^{\mathrm{t}},\ \bar{\boldsymbol{\varepsilon}}_{\mathrm{b}}^{\mathrm{t}},\ \bar{\boldsymbol{\varepsilon}}_{\mathrm{s}}^{\mathrm{t}}) \tag{4g}$$

3. Finite element formulation

The finite element used here is a nine noded quadrilateral element belonging to the Lagrangian family. The laminate displacement field in the element can be expressed in terms of nodal variables as

$$\boldsymbol{d}(\xi, \eta) = \sum_{i=1}^{\mathrm{NN}} N_i(\xi, \eta) \cdot \boldsymbol{d}_i \tag{5}$$

where NN is a number of nodes per element, $N_i(\xi, \eta)$ contains interpolation functions associated with

node i in terms of local coordinates ξ, η and $\boldsymbol{d}_i$ is nodal displacement vector such that $\boldsymbol{d}_i^{\mathrm{t}} = (u_{0i}, v_{0i}, w_{0i}, \theta_{xi}, \theta_{yi}, u_{0i}^*, v_{0i}^*, \theta_{xi}^*, \theta_{yi}^*)$. The strain–displacement relations can be written as follows [2]

$$\bar{\boldsymbol{\varepsilon}} = \left(\boldsymbol{B}_0 + \frac{1}{2}\boldsymbol{B}_{\mathrm{NL}}\right) \cdot \boldsymbol{a} \tag{6a}$$

$$\delta\bar{\boldsymbol{\varepsilon}} = (\boldsymbol{B}_0 + \boldsymbol{B}_{\mathrm{NL}}) \cdot \delta\boldsymbol{a} \tag{6b}$$

$$\delta\bar{\boldsymbol{\varepsilon}} = \sum_{i=1}^{\mathrm{NN}} \mathbf{B}_i \cdot \delta\boldsymbol{d}_i = \boldsymbol{B}\,\delta\boldsymbol{a} \tag{6c}$$

where $\boldsymbol{B}_0$ is the strain matrix giving linear strains, $\boldsymbol{B}_{\mathrm{NL}}$ is linearly dependent upon the nodal displacement vector $\boldsymbol{a}$, such that $\boldsymbol{a}^{\mathrm{t}} = (\boldsymbol{d}_1^{\mathrm{t}}, \boldsymbol{d}_2^{\mathrm{t}}, \ldots, \boldsymbol{d}_{\mathrm{NN}}^{\mathrm{t}})$. The non-zero coefficients of the $\boldsymbol{B}_i$ sub-matrix are defined as follows

Membrane and flexure terms (size of matrix, 12×9):

$$B_{1,1} = B_{3,2} = B_{4,6} = B_{6,7} = B_{7,4} = B_{9,5} = B_{10,8} = B_{12,9} = \frac{\partial N_i}{\partial x}$$

$$B_{2,2} = B_{3,1} = B_{5,7} = B_{6,6} = B_{8,5} = B_{9,4} = B_{11,9} = B_{12,8} = \frac{\partial N_i}{\partial y}$$

$$B_{1,3} = \frac{N_i}{R_1} + \frac{\partial w_0}{\partial x} \cdot \frac{\partial N_i}{\partial x}; \qquad B_{2,3} = \frac{N_i}{R_1} + \frac{\partial w_0}{\partial y} \cdot \frac{\partial N_i}{\partial y}; \qquad B_{3,3} = \frac{\partial w_0}{\partial x} \cdot \frac{\partial N_i}{\partial y} + \frac{\partial w_0}{\partial y} \cdot \frac{\partial N_i}{\partial x}$$

Shear terms (size of matrix, 8×9):

$$B_{1,3} = \frac{\partial N_i}{\partial x}; \qquad B_{2,3} = \frac{\partial N_i}{\partial y}; \qquad B_{1,4} = B_{2,5} = N_i;$$

$$B_{3,8} = B_{4,9} = 3N_i; \qquad B_{5,6} = B_{6,7} = 2N_i$$

$$B_{1,1} = B_{3,6} = B_{5,4} = B_{7,8} = -\frac{N_i}{R_1}; \qquad B_{2,2} = B_{4,7} = B_{6,5} = B_{8,9} = -\frac{N_i}{R_2} \tag{7}$$

The discrete static equilibrium equations can be written as

$$\boldsymbol{P}(a, t) = \boldsymbol{f} \tag{8a}$$

and the discrete dynamic equations of motion as

$$\boldsymbol{P}(a, t) + \boldsymbol{C}\dot{\boldsymbol{a}} + \boldsymbol{M}\ddot{\boldsymbol{a}} = \boldsymbol{f} \tag{8b}$$

The static problem represented by the discrete equation (8a) can be solved in a variety of ways. This generally requires a direct or a factorized solution of simultaneous equations. An alternate solution procedure includes the transformation of Eq. (8a) into a dynamic equation of motion represented by Eq. (8b) by inclusion of fictitious mass and/or damping matrices and carrying out the dynamic analysis until the steady state is reached. In the above equation, $\boldsymbol{M}$ is the mass matrix, $\boldsymbol{C}$ is the damping matrix, $\boldsymbol{P}(a, t)$ is the vector of internal resisting forces, $\boldsymbol{f}$ is the vector of applied forces, $\boldsymbol{a}$ is the vector of nodal displacements and a dot denotes differentiation with respect to the time. The matrices/vectors in Eq. (8b) are defined as

(a) Internal force vector $\boldsymbol{P}$:

$$\boldsymbol{P}(a, t) = \int_A \boldsymbol{B}^{\mathrm{t}} \bar{\boldsymbol{\sigma}}\, \mathrm{d}A \tag{9}$$

where $\bar{\boldsymbol{\sigma}}$ is a stress-resultant vector.

(b) Mass matrix $\boldsymbol{M}$:

In the pseudo-transient analysis the real mass is very seldom used. In the present investigation the

diagonal terms of the linear stiffness matrix are taken as diagonal coefficients of diagonal fictitious mass matrix.

(c) Damping matrix $\boldsymbol{C}$:

In the present investigation the damping matrix is taken as

$$\boldsymbol{C} = \alpha_c \cdot \boldsymbol{M} \tag{10a}$$

where α_c is the critical damping factor, such that $\alpha_c = 2 \cdot \omega$ in which ω is the dominant frequency of the system. An eigenvalue analysis of the system for evaluating ω is generally avoided. In fact it would be rather expensive and contrary to the main philosophy of pseudo-transient methods in which the aims are easy implementation and small computer core storage. In the present context the damping effect is included by considering the kinetic damping. In this the variation of the total kinetic energy during some non-productive steps is used for estimating the period of vibration of the structure, i.e. the time employed by the structure to reach the maximum total kinetic energy is estimated through the variation of the total kinetic energy and is assumed as one fourth of the period of vibration and consequently, the critical damping factor α_c is given by

$$\alpha_c = 2 \cdot \omega = 4 \frac{\pi}{T} \tag{10b}$$

The same damping factor is applied till the structure attains a steady-state.

An alternate procedure, called an adaptive damping, in which the damping factor is constantly updated on the basis of the information gained during the current time step is also considered here. It is thus possible to follow the behaviour of the structure during the integration in time much closely than the kinetic damping. It consists of using the Raleigh's quotient

$$\lambda_n = \left[\frac{\boldsymbol{a}_n^{\mathrm{t}} \boldsymbol{K} \boldsymbol{a}_n}{\boldsymbol{a}_n^{\mathrm{t}} \boldsymbol{M} \boldsymbol{a}_n} \right]^{1/2} \tag{11}$$

as an estimate of lowest eigenvalue of the structure at the current time step.

Since the mass matrix $\boldsymbol{M}$ and damping matrix $\boldsymbol{C}$ are diagonal matrices, the set of equations (8b) are uncoupled and give displacement values at a time stage without requiring matrix factorization or any sophisticated solution techniques. Eqs. (8b) can be written in a scalar form as [3]

$$m_i \ddot{a}_i + c_i \dot{a}_i + p_i = f_i \tag{12}$$

where subscript 'i' denotes the ith degree of freedom and the other symbols have usual meanings.

In the explicit time marching scheme used here the velocities and accelerations are approximated using the central difference formulae as

$$\dot{a}_i^n = (a_i^{n+1} - a_i^{n-1})/2 \cdot \Delta t \tag{13a}$$

$$\ddot{a}_i^n = (a_i^{n+1} - 2 \cdot a_i^n + a_i^{n-1})/\Delta t^2 \tag{13b}$$

where $n-1, n, n+1$ denote three successive time stations. Using the above approximation, Eq. (12) can be rewritten as

$$m_i \cdot (a_i^{n+1} - 2 \cdot a_i^n + a_i^{n-1})/\Delta t^2 + c_i \cdot (a_i^{n+1} - a_i^{n-1})/2\,\Delta t + p_i^n - f_i^n = 0 \tag{14}$$

It becomes clear that the values of a_i^{n+1} can be determined from the two previous displacements, a_i^n and a_i^{n-1} by rewriting Eq. (14) as

$$a_i^{n+1} = \left(m_i + c_i \frac{\Delta t}{2} \right)^{-1} \left(\Delta t^2 (f_i^n - p_i^n) + 2 m_i \cdot a_i^n - \left(m_i - c_i \frac{\Delta t}{2} \right) \cdot a_i^{n-1} \right) \tag{15a}$$

If the values a^0 and $\dot{a}^0$ are specified as initial conditions, a special starting algorithm can be written by noting that

$$\dot{a}_i^0 = (a_i^1 - a_i^{-1})/2 \cdot \Delta t \tag{15b}$$

and a_i^{-1} can be eliminated from Eq. (15a).

The algorithm defined by Eqs. (15a) and (15b) is very simple and easy to implement, but as is well known, it is conditionally stable. This means that the time step length Δt must not exceed a given critical value for the scheme to be stable. The critical time step Δt_{cr} can be shown to be equal to 1.0 and 0.5 for thin ($a/h = 100$) and moderately thick ($a/h = 10$) laminates respectively regardless of spatial finite element mesh.

4. Numerical examples and discussion

The validity and suitability of the present unified approach for composite and sandwich shells can be investigated by considering and evaluating a set of benchmark problems. Two computer programs are developed: one is based on higher-order shear deformation theory (PTHOST) and the other one on first-order shear deformation theory (PTFOST). The bi-quadratic nine-noded Lagrangian isoparametric element is employed in the numerical evaluations. The selective integration scheme namely 3×3 Gauss quadrature rule is used to integrate the membrane, coupling between membrane and bending and bending energy terms and a 2×2 Gauss quadrature rule is used to integrate shear energy terms. Zero initial conditions are assumed in all the examples of pseudo-transient analysis. All the computations were carried out in single precision on CDC Cyber 180/840 computer at Indian Institute of Technology, Bombay. Due to bi-axial symmetry of the problems discussed only one quadrant of shell was analyzed with a 2×2 uniform mesh except angle-ply shells where the full shell with a 4×4 uniform mesh is adopted. A convergence study was first undertaken in the beginning with a view to assess the type and nature of discretization required for reliable converged results. It was seen that with nine-node Lagrangian quadrilateral elements, a 2×2 mesh (4 elements) in a quarter laminate and a 4×4 mesh (16 elements) in a full laminate were sufficient for getting converged solution for displacements and lamina tangential stresses for all geometrical configurations, boundary and loading conditions considered in this paper. In the present investigation unless otherwise specified, the following material properties are used.

$$E_1 = 25E_2\,; \quad G_{12} = G_{13} = 0.5E_2\,; \quad G_{23} = 0.2E_2\,; \quad \nu_{12} = \nu_{23} = \nu_{13} = 0.25$$

EXAMPLE 1: Linear analysis. To the authors' knowledge, there exists no available 3D elasticity solutions in non-linear context. To show the superiority of present higher order theory over first order shear deformation theory, a problem which had 3D elasticity solution in the linear context was analyzed [4].

A symmetric 3-ply cylindrical shell of infinite length with radius of 10 in, arc length of 10.472 in and layers of equal thick subjected to a sinusoidal transverse load of $q_0 = q_0 \sin(\pi s_1/s)$ is considered [4, 5]. The boundaries are free along circumferential direction and simply supported along longitudinal direction. The material T-direction coincides with the θ direction in outer layers while the material L-direction is parallel to the θ direction in the central layer. A 1×10 ($X \times \theta$-directions) discretization for one quarter of the shell gives converged results. The transverse displacement $\hat{w}_0$ and the circumferential stresses are taken at the center of shell. The results are presented in Table 1. The following non-dimensional quantities are used to present the results

$$\hat{w}_0 = \left(\frac{h^3 E_2}{p_0 R^4} \times 10\right) \cdot w_0\,; \qquad \hat{\sigma}_\theta = \left(\frac{h^2}{p_0 R^2}\right) \cdot (\sigma_\theta) \tag{16}$$

Dennis and Plazotto [5] have adopted a higher-order displacement model, which satisfies the shear free boundary condition on the bounding surfaces of shell. From the results of Table 1, it is clear that present higher-order shear deformation theory predictions are very close to 3D elasticity results in comparison with another higher-order shear deformation theory and first-order shear deformation theory. The higher-order shear deformation theory presented by Dennis and Plazotto [5] gives stiffer solutions. This may be due to the imposition of shear free conditions on the bounding surfaces. The classical shell theory (CST) predictions are very poor especially in thick zones.

Table 1
Transverse displacement and extreme fibre circumferential stresses at the middle of an infinite long cylindrical cross-ply (0°/90°/0°) shell subjected to a sinusoidal transverse load

R/h	Variable	Exact3D[4] elasticity	HSDT [5]	CST [5]	PTFOST	PTHOST
4	$\hat{w}_0$	0.4570	0.382	0.078	0.036	0.4087
	$\hat{\sigma}_{\theta b}$	1.7720	1.406	0.824	0.824	1.3636
	$\hat{\sigma}_{\theta t}$	1.3670	1.117	0.732	0.721	1.2980
10	$\hat{w}_0$	0.1140	0.128	0.078	0.123	0.1350
	$\hat{\sigma}_{\theta b}$	0.9950	0.889	0.796	0.792	0.8910
	$\hat{\sigma}_{\theta t}$	0.8970	0.829	0.759	0.751	0.8710
50	$\hat{w}_0$	0.0810	0.079	0.077	0.075	0.0797
	$\hat{\sigma}_{\theta b}$	0.7980	0.789	0.792	0.792	0.7912
	$\hat{\sigma}_{\theta t}$	0.7820	0.774	0.774	0.761	0.7714
100	$\hat{w}_0$	0.0787	0.078	0.078	0.071	0.0761
	$\hat{\sigma}_{\theta b}$	0.7860	0.787	0.779	0.791	0.7941
	$\hat{\sigma}_{\theta t}$	0.7810	0.770	0.776	0.751	0.7631

To show the validity further the present results are compared with the corresponding closed-form solutions presented by Reddy and Liu [6]. A simply supported cross-ply (0°/90°) spherical shell subjected to a uniform/sinusoidal transverse load is considered. The results are compared with Reddy and Liu [6] and are presented in Table 2. The non-dimensional quantity for representing displacement is as follows,

$$\hat{w}_0 = \left(\frac{h^3 E_2}{q_0 a^4} - \times 10^3\right) w_0 \tag{17}$$

From the above results it is clear that all the theories predict the same results in the case of geometrically thin shells, but as the thickness increases the classical thin shell theory (CLT) and first-order shear deformation theory (PTFOST) underpredict displacements. Whereas present PTHOST

Table 2
Transverse displacement in a simply supported cross-ply (0°/90°) spherical shell subjected to a sinusoidal/uniform transverse loads

R/a	Theory	Sinusoidal transverse load				Uniform transverse load			
		$a/h = 100$		$a/h = 10$		$a/h = 100$		$a/h = 10$	
		CFS [6]	Present	CFS [6]	Present	CFS [6]	Present	CFS [6]	Present
5	FOST	1.1948	1.1913	11.429	11.4300	1.7535	1.7525	19.944	17.9668
	HOST	1.1937	1.1913	11.166	11.1846	1.7519	1.7526	17.566	17.7003
10	FOST	3.5760	3.5674	12.123	12.1299	5.5428	5.5369	19.065	19.0920
	HOST	3.5733	3.5673	11.896	11.8925	5.5388	5.5369	18.744	18.8933
20	FOST	7.1270	7.1195	12.309	12.3106	11.2730	11.2757	19.365	19.3872
	HOST	7.1236	7.1189	12.094	12.1449	11.2680	11.2749	19.064	19.0912
50	FOST	9.8717	9.8731	12.362	12.3684	15.7140	15.7361	19.452	19.4638
	HOST	9.8692	9.8713	12.150	12.2271	15.7110	15.7372	19.155	19.1753
100	FOST	10.4460	10.4500	12.370	12.3709	16.6450	16.6737	19.464	19.4763
	HOST	10.4440	10.4493	12.158	12.2301	16.6420	16.6597	19.168	19.1874
Plate	FOST	10.6530	10.6533	12.373	12.3704	16.9800	17.0015	19.469	19.5004
	HOST	10.6510	10.6539	12.161	12.2301	16.9770	17.0016	19.172	19.1914

predicts the displacement and stresses very close to the 3D elasticity results. This indicates that as the shear deformation effect increases, the present simple C^0 higher-order finite element theory is the best alternate to the classical thin shell theory and first-order shear deformation theory.

EXAMPLE 2: Isotropic cylindrical shell. A clamped isotropic cylindrical shell with $a = b = 508$ mm, $h = 3.175$ mm, $R = 2540$ mm, $E = 3.103$ KN/mm^2 and $\nu = 0.3$ subjected to a uniform transverse load is considered. The present results are compared with Dhatt [7] and Reddy and Chandrashekhara [8] and are presented in Figs. 2(a) and (b). The present results match very well with solutions given by others. The limitation of this comparison is that the shell considered is geometrically thin with negligible shear deformation effects. However, this comparison has certainly proved the validity of the present formulation in the non-linear context.

EXAMPLE 3: Sandwich spherical shell. A clamped angle-ply sandwich (0°/45°/90°/CORE/90°/45°/30°/0°) spherical shell of $R/a = 10$ subjected to a uniform transverse load is considered. The geometry and material properties are as follows

$a = b = 100$ cm

For face sheets, the assumed ply data is based on Hercules ASI/3501-6/graphite/epoxy prepreg system

$$E_1 = 13.08 \times 10^6 \text{ N/cm}^2, \quad E_2 = E_3 = 1.06 \times 10^6 \text{ N/cm}^2$$
$$G_{12} = G_{13} = 0.6 \times 10^6 \text{ N/cm}^2, \quad G_{23} = 0.39 \times 10^6 \text{ N/cm}^2,$$
$$\nu_{12} = \nu_{13} = 0.28, \quad \nu_{23} = 0.34$$

Thickness of each top stiff layer = 0.025h
Thickness of each bottom stiff layer = 0.08125h
Core material is of U.S. commercial aluminum honeycomb (1/4 inch cell size, 0.003 inch foil)

$$G_{23} = 1.772 \times 10^4 \text{ N/cm}^2, \quad G_{13} = 5.206 \times 10^4 \text{ N/cm}^2$$
$$E_3 = 3.013 \times 10^5 \text{ N/cm}^2$$

Thickness of core = 0.6 h

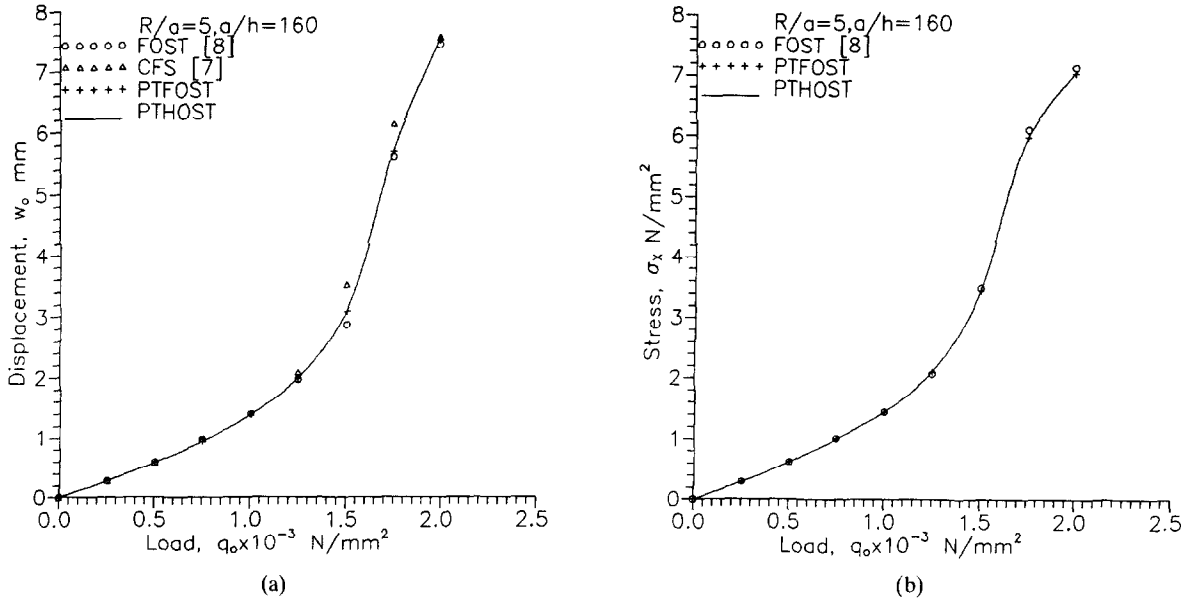

(a) (b)

Fig. 2. (a) Displacement vs. load curves for a clamped cylindrical isotropic shell subjected to a uniform transverse load; (b) Stress vs. load curves for a clamped cylindrical isotropic shell subjected to a uniform transverse load.

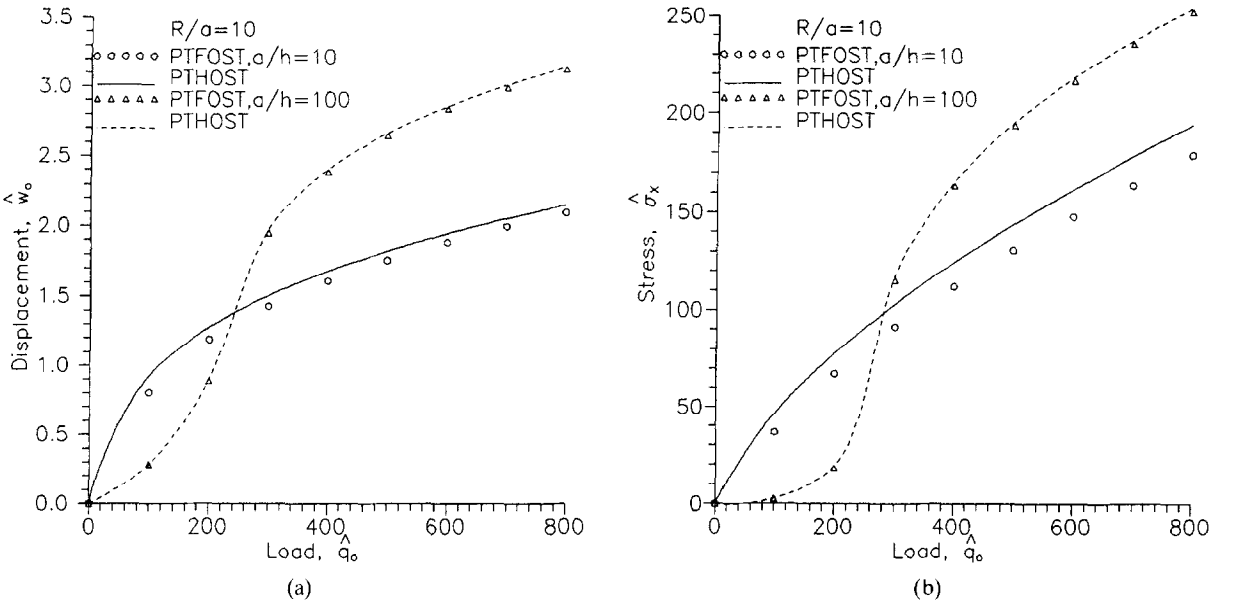

Fig. 3. (a) Displacement vs. load curves for a clamped angle-ply sandwich (0°/45°/90°/core/90°/45°/30°/0°) spherical shell subjected to a uniform transverse load; (b) Stress vs. load curves for an angle-ply sandwich (0°/45°/90°/core/90°/45°/30°/0°) spherical shell subjected to a uniform transverse load.

The non-dimensional quantities are defined as follows

$$\hat{w}_0 = \left(\frac{w_0}{h}\right) \qquad \hat{q}_0 = \frac{q_0}{E_2}\left(\frac{a}{h}\right)^4 \qquad \hat{\sigma}_x = \frac{\sigma_x}{E_2}\left(\frac{a}{h}\right)^2 \tag{18}$$

The results for displacement and extreme fibre stresses are presented in Figs. 3(a) and (b) for different side to thickness ratios. It is observed that for $a/h = 100$, the results predicted by first-order shear deformation (PTFOST) and higher-order shear deformation theory (PTHOST) are almost same, whereas for $a/h = 10$, the results predicted by PTHOST and PTFOST differ considerably. This is due to predominant shear deformation leading to warping of transverse sections. In earlier examples it was proved that as shear deformation effect increases, the results predicted by PTHOST are more reliable.

EXAMPLE 4: Time history of displacement for an angle-ply shell. A simply supported angle-ply (45°/−45°) spherical shell with $a/h = 10$ and 100 subjected to a sinusoidal transverse load of intensity $\hat{q}_0 = 900$ is considered. In the case of thick shell, damping is included by considering adaptive damping in which the damping factor is constantly updated on the basis of information gained in the current time step. The time history of transverse displacement is plotted in Fig. 4(a). For thin shell, damping effects are included by considering kinetic damping and the corresponding time history is shown in Fig. 4(b). Steady-state values of 1.87858 and 3.60734 are, respectively, obtained as against the corresponding static Newton–Raphson (NR) approach results of 1.85362 and 3.60734 for thick and thin shells given in [9].

After doing rigorous numerical computations with different damping factors for thin and thick shells, it is observed that system reaches steady state quickly with kinetic damping and adaptive damping respectively.

EXAMPLE 5: Comparison of solution algorithms. A simply supported angle-ply (45°/−45°) spherical shell with $a/h = 10$ and 100 subjected to a sinusoidal transverse load is considered. The non-dimensionalization of load is as per relations (18). The spot analysis technique (i.e. the total load is imposed in one increment) is adopted. Furthermore, the pseudo-transient (PT) analysis is performed using fictitious mass matrix with a time step small enough to preserve the stability at larger loads.

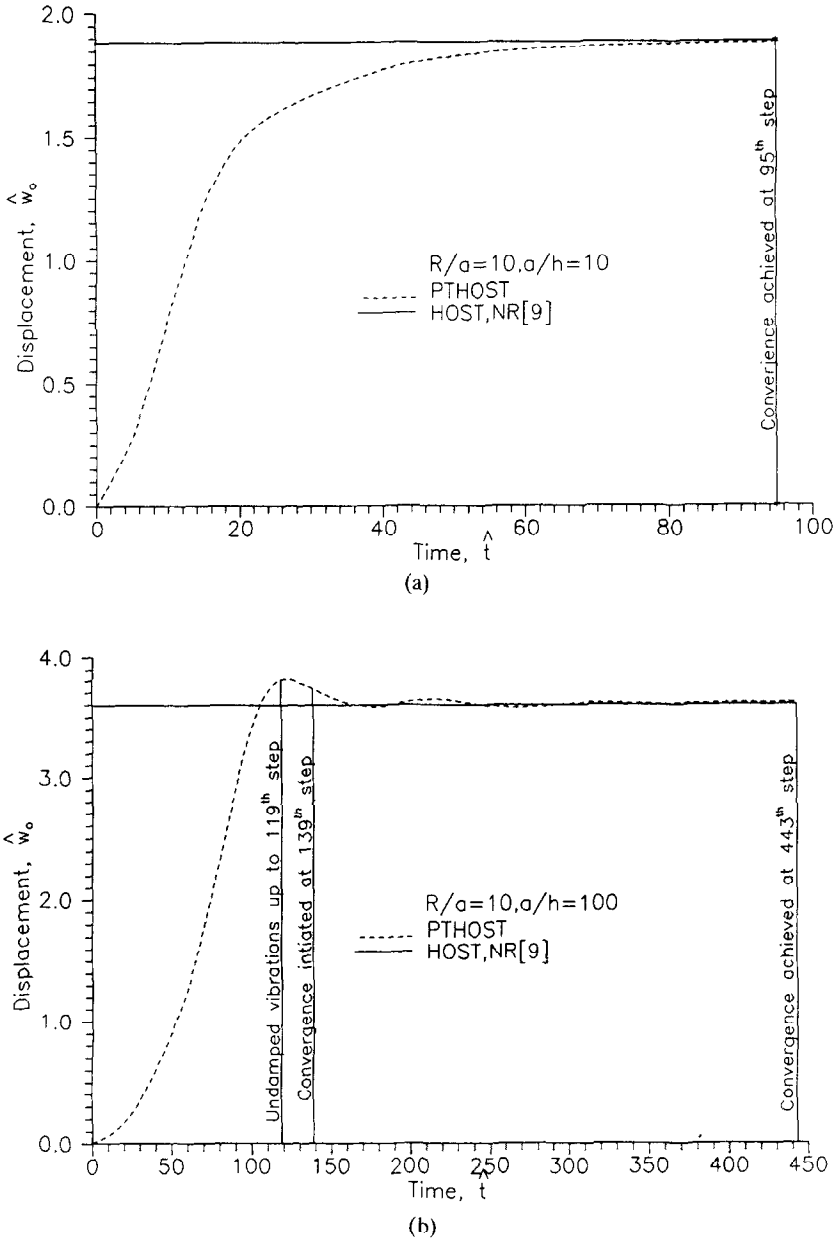

Fig. 4. (a) Time history of displacement for a simply supported angle-ply (45°/−45°) spherical shell subjected to a sinusoidal transverse load with adaptive damping (Thick shell); (b) Time history of displacement for a simply supported angle-ply (45°/−45°) spherical shell subjected to a sinusoidal transverse load (Thin laminate, $a/h = 100$) with kinetic damping.

The results are presented in terms of CPU time (in seconds) required on CDC Cyber 180/840 for the solution to converge within a tolerance of 1 percent residual forces.

The sensitivity of this method to varying degrees of non-linearities is studied by taking different intensities of loads producing a maximum non-linear deflection at the center of laminate in the range of h to $3h$. The results are plotted in Figs 5(a) and (b). The behaviour of the present pseudo-transient analysis for thick and thin shells is different. The performance of PT method for thin shells under large loads is greatly improved whereas for thick shells the over-all performance is generally improved under all magnitudes of loads. From Figs. 5(a) and (b) it is clear that the additional computational time required with higher-order theory over first-order theory is far less in PT method in comparison with Newton–Raphson (NR) method. It is due to the fact that only internal force vector needs to be

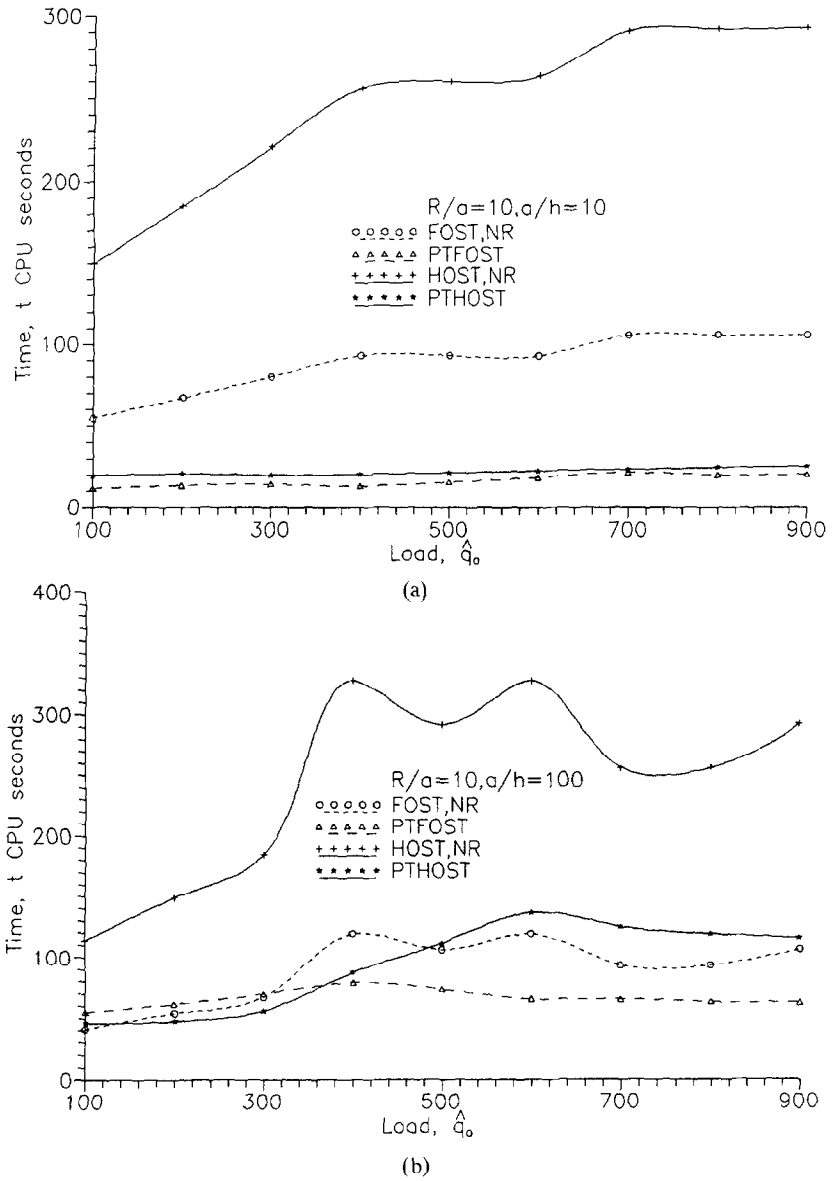

Fig. 5. (a) Comparison of computational time: A simply supported angle-ply (45°/−45°) spherical shell subjected to a sinusoidal transverse load with adaptive damping (Thick shell); (b) Comparison of computational time: A simply supported angle-ply (45°/−45°) spherical shell subjected to a sinusoidal transverse load with kinetic damping (Thin shell).

computed in PT method whereas the Newton–Raphson method needs not only computation of internal force vector but also factorization of static equilibrium equations. It is thus clearly seen that the PT method is computationally efficient especially in the case of thick shells. Furthermore, there is not much difference in computational time in PT method for different intensities of load while in Newton–Raphson method, the computational time requirement increases as load increases.

4. Conclusions

The pseudo-transient analysis methodology based on finite element space discretization is an adaptation of the dynamic relaxation methodology based on finite difference space discretization originally developed in 1965 for solution of both linear and non-linear problems in an unified manner.

A comparison of this method with the standard Newton–Raphson method for solution of the non-linear equations of a problem under consideration is not available in literature. An effort in this direction is made here in the context of large deflection elasto-static problems of general fibre reinforced composite shells.

The numerical examples presented in Section 3 show a good correlation. This unified approach is seen to be working equally well for both linear and geometrically non-linear problems of isotropic/orthotropic and anisotropic material properties with any extent of non-linearity. It is important to note that the computer code requires very small core memory as compared to static programs. It is further noted that this method enables solution of very large linear and non-linear finite element problems on small computers. Another important merit of the present unified approach is its easy implementation.

It is observed that the effect of shear deformation in thick sandwich shells with weak core and strong facings as well as laminated shells with large ratios of the tangential elastic modulus to the transverse shear modulus is considerable. It is believed that the refined shear deformation theory presented herein is essential for predicting accurate responses especially for thick composite and sandwich shells.

Acknowledgment

Partial support of this research by the Aeronautics Research and Development Board, Ministry of Defense, Government of India through its Grant Nos. Aero/RD-134/100/10/88–89/518 and Aero/RD-134/100/10/88–89/534 is greatly acknowledged.

References

[1] B.N. Pandya and T. Kant, Flexural analysis of laminated composites using refined higher order C^0 plate bending elements, Comput. Methods Appl. Mech. Engrg. 66 (1988) 173–198.

[2] O.C. Zienkiewicz, The Finite Element Method, 3rd edition (McGraw-Hill, London, 1977).

[3] Mallikarjuna and T. Kant, Finite element transient responses of composite and sandwich plates with a refined theory, ASME J. Appl. Mech. 57 (1990) 1084–1086.

[4] J.G. Ren, Exact solutions for laminated cylindrical shells in cylindrical bending, Composite Sci. and Tech. 32 (1987) 137–155.

[5] S.T. Dennis and A.N. Plazotto, Laminated shell cylindrical bending, Two-dimensional approach vs. Exact, AIAA J. 29 (1991) 647–650.

[6] J.N. Reddy and C.F. Liu, A higher-order shear deformation theory of laminated elastic shells, Int. J. Engrg. Sci. 23 (1985) 319–330.

[7] G.S. Dhatt, In-stability of thin shells by finite element method, IASS Symposium for Folded Plates and Prismatic Structures, Vienna, 1970.

[8] J.N. Reddy and K. Chandrashekhara, Non-linear analysis of laminated shells including transverse shear strains, AIAA J. 23 (1985) 440–441.

[9] T. Kant and J.R. Kommineni, Geometrically non-linear analysis of doubly curved laminated and sandwich fibre reinforced composite shells with a higher order theory and C^0 finite elements, J. Reinforced Plastics and Composites 11 (1992) 1048-1076.